CHEMISTRY OF MATERIALS

Article

pubs.acs.org/cm

Anionic Dopants for Improved Optical Absorption and Enhanced Photocatalytic Hydrogen Production in Graphitic Carbon Nitride

Stephen A. Shevlin* and Zheng Xiao Guo*

Department of Chemistry, University College London, Gower Street, London WC1E 6BT, United Kingdom

ABSTRACT: Graphitic carbon nitride is an exemplar material for metal-free photocatalytic hydrogen production, essential to drive the change to a greener economy. However, its bandgap is too large, at 2.7 eV, for visible light harvesting, which hinders uptake in applications. From two sets of independent quantum mechanical simulations, we have determined the effect of two representative interstitial (hydrogen and fluorine) dopants on the electronic structure and optical properties of this material. From defect analysis, we have found that for a significant range of chemical potential the anionic fluorine dopant is favored. This dopant has significant effects on the optical absorption with the valence band edge shifted up by 0.55 eV, which extends light absorption into the visible. In contrast, hydrogen prefers to be cationic, with the conduction band edge shifted down by 0.45 eV, which strongly reduces hydrogen production as the thermodynamic driving force for proton reduction is significantly reduced. Fluorine is advantageous for improved H_2 production as band gap reduction is driven by raising of the valence band, with minimal effect on the thermodynamic driving force for hydrogen reduction. We propose that a design principle for improving carbon nitrides for hydrogen production is to use strongly electronegative dopants.

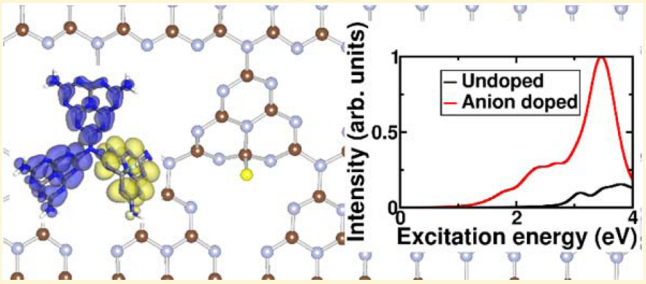

INTRODUCTION

Low cost and effective hydrogen (H_2) production via photocatalysis of water is urgently required to leverage the free energy of the sun to synthesize clean renewable fuel. Since the discovery of photocatalytic water-splitting and hydrogen production,[1] many inorganic semiconductors have been found to photocatalyze H_2 production from water including oxides,[2] sulfides,[3] and oxynitrides.[4] Furthermore, semiconductor heterojunctions have been demonstrated to also be viable for hydrogen production.[5] Much success has been achieved with these materials or structures, but to meet industrial requirements, significant improvements must be made in stability, cost, and efficiency. Organic photocatalysts would meet many of these requirements and with their diverse synthetic modularity provide plenty of options for tailoring of electronic and optical properties.[6]

Graphitic carbon nitride (g-C_3N_4) is an exemplar organic photocatalyst, composed purely of nontoxic and plentiful elements, which dissociates water and generates H_2 under (short wavelength) visible light.[7] However, long wavelength light absorption is poor due to the large optical gap of 2.7 eV, which limits quantum efficiency and prevents its direct application. Modification and chemical doping of semiconductors are well-developed methods for altering the electronic structure and thus the optical properties. The presence of carbon or nitrogen vacancies, with formation energies of ∼0.08−2.09 eV, reduces the optical band gap but results in shallow and deep traps that promote exciton recombination, which reduce the photocurrent.[8] Modification of the lattice parameter has been theoretically demonstrated to significantly alter the optical band gap, with reduction of the in-plane lattice parameter from a ∼7.3 Å to ∼6.8 Å, which results in a band gap reduction of approximately an electronvolt due to a reduction in the energy of unoccupied p_z orbitals.[9] Experimental realization of compression-induced bandgap reduction and associated optical absorption deeper into the visible range will only occur for carbon nitrides grown on substrates such as scandium, which limits their applicability for cheap photocatalysts. Several different prospective dopants have been studied to improve the optical absorption by reduction of the band gap. This includes nitrogen,[10] oxygen,[11] boron,[12,13] phosphorus,[14] sulfur,[15−17] iron,[18] iodine,[19] fluorine,[20−22] and precursors infiltrated with methyl orange dyes,[23] or 2,6-diaminopyridine.[24] Additional nitrogen atoms can dope into carbon lattice sites, which results in a minor decrease of the band gap of less than 0.1 eV (from 2.72−2.65 eV).[10] A greater reduction in the bandgap is observed for oxygen-doping, with a reduction of 0.21 eV measured experimentally.[11] This is believed to arise from oxygen atom insertion on a nitrogen site, which results in a lowering of bandgap position due to the formation of a partially empty occupied state ∼0.22 eV below the conduction band edge (CBE).[25] Boron doping was found to improve the photocatalytic activity of g-C_3N_4 toward rhodamine B photo-oxidation, partially associated with a reduction of the band gap by 0.04 eV and, furthermore, by also providing a reaction site for photocatalysis.[12,13] Sulfur

Received: May 18, 2016
Revised: September 14, 2016
Published: September 14, 2016

doping was demonstrated to result in an approximate order of magnitude increase in the H_2 production rate under UV (300 nm) and visible (420 nm) light.[17] This is despite an increase in the band gap of 0.12 eV, caused by an upward shift of the CBE. The posited mechanism behind the increase in H_2 production is that the CBE moves toward the vacuum level, which increases the thermodynamic driving force for H+/H reduction. Density functional theory (DFT) simulation, which uses the generalized gradient approximation functional, found that direct insertion of sulfur dopants into nitrogen sites is of relatively low energy, with an endothermic formation energy of 0.47 eV for the +1 charge state,[15] in agreement with experiment.[16] Phosphorus dopants were found to increase the photocurrent, and thus the photoactivity, by a factor of 5. The electronic structure was modified, with DFT simulations indicating that the phosphorus atoms are present as interstitials in the carbon nitride lattice. This suggests that the formation of deep defect levels will provide easily accessible conduction pathways for charge carriers near the Fermi level, thus increasing the conductivity.[15] Iodine dopants induce a long tail in the optical absorption region, from 420−600 nm, with an associated doubling in the H_2 evolution rate.[19] This is ascribed to iodine dopants inserting into the carbon nitride heterocycle. Fluorination of carbon nitrides results in an increase in the optical absorption, with a band gap decrease of 0.06 eV, where the F dopant was assumed to dope into the crystal lattice.[20,21] Further experimental work by Wang et al. found a slight increase in the bandgap of 2.8 eV.[22] However, the photocatalytic activity is improved, ascribed to a mechanism whereby fluorine induces structural distortions that enhance charge separation.

Many dopants for g-C_3N_4 have been investigated. The majority of them do not reduce the band gap by more than 0.2 eV (corresponding to an increase in the onset for optical absorption of ∼45 nm). This is a relatively minor improvement. Furthermore, many of the dopants directly insert into the C−N heterostructure, with implications for the delocalized π-states and the charge transport properties. Finally, many dopants modify the conduction band edge position, with implications for the H+/H redox reaction. Specifically, if the bandgap is reduced via lowering of the CBE, the thermodynamic driving force for proton reduction is reduced, which thus reduces the kinetics of H_2 production. We have already demonstrated that protonation of carbon nitride hinders H_2 production due to this effect and that a synthesis can be developed to minimize the proton concentration, which thus results in an optimized carbon nitride.[26] The implications of our previous work are that dopants that raise the valence band edge (VBE) and do not modify the CBE will be significantly better for H_2 production, as the photoabsorption is improved while the thermodynamic driving force for proton reduction is not altered. In particular, this suggests that anion doping in particular is ideal for this purpose, as for most charge transfer ionic semiconductors the VBE is dominated by the anion.

Building on the knowledge gained in our previous work, we simulate, using both hybrid DFT and time dependent DFT, the effects of two exemplar contrasting interstitial dopants on the electronic and optical properties of g-C_3N_4. These dopants are the cationic dopant hydrogen (with a strong tendency to become cationic) and the anionic dopant fluorine (with a strong tendency to become anionic). We demonstrate that both dopants bind significantly to the heterostructure without strongly modifying the lattice. We show that, for fluorine doping, F anions are energetically favorable over a large part of the electron chemical potential. However, for hydrogen doping, H cations are energetically favorable over a large part of the electron chemical potential. We further demonstrate that this has important implications for the band gap and thus the electronic properties. For hydrogen-doped systems it is likely that photocatalytic H_2 production is quenched due to the detachment of a low-lying empty state near the CBE. In contrast, we show that fluorine anion dopants are beneficial for H_2 production due to the creation of a raised occupied state near the VBE that reduces the bandgap by 0.45 eV. Furthermore, we use time dependent density functional theory (TDDFT) calculations to determine the exciton distribution and find that the exciton is not strongly localized and pinned onto the dopants, with photoholes and photoelectrons able to participate in chemical reactions.

METHODS

Hydrogen and fluorine interactions with carbon nitride were investigated using both periodic and large-scale cluster models. For periodic models, we used the VASP code.[27] A plane wave cutoff of 520 eV was selected, with the projector augmented wave methods used to treat the core electrons.[28] Initial relaxation was performed using the PBESol exchange correlation functional,[29] with final geometry optimization and electronic structure analysis performed using the HSE06 functional.[30] This functional has been found to be highly accurate in determining structures and bandgaps.[31] All atoms were fully relaxed until the change in force upon ionic displacement was less than 0.01 eV/Å, with the change in energies no greater than 10^{-5} eV. The lattice parameters of the unit cell of g-C_3N_4 were obtained by generating energy−volume data from a series of constant volume cell shape optimization calculations and fitting this data to the Murnaghan equation of state. Final lattice parameters of a = 6.9157 Å, b = 6.9022 Å, and c = 7.7371 Å were obtained. Our value for a is in very close agreement with the experimentally measured value of 6.91 Å reported by Wang et al.[18] Since there is no treatment of van der Waals forces in our calculations, our value for c is an overestimate. However, when we checked our calculations using the van der Waals treatment of Grimme, we found that there were only minor corrections to c, of order 0.6%. The structural changes do not have a significant effect on the electronic structure, with very little change in the bandgap. The effects of dopants on the electronic structure were modeled using the supercell approach, with the supercells consisting of $(2 \times 2 \times 1)$ unit cells, while a Monkhorst−Pack k-point mesh of $(2 \times 2 \times 1)$ was found to be sufficient to produce well converged energies and forces. We arranged our sheets in a AB stacking arrangement, to fully represent the graphitic layered structure of g-C_3N_4,[32] and in agreement with simulations that indicate this is the lower energy stacking order.[8,33] This arrangement also allows the minimization of dopant−dopant interactions along the c-axis. Since both F- and H-doped supercells have an odd number of electrons, spin polarization was used in all of our calculations.

For cluster models, we used the Gaussian-based NWChem code[34] and the 6-311G** basis set.[35,36] We approximated amorphous carbon nitride structures with a cluster composed of three heptazine rings, with each corner nitrogen passivated by two hydrogens, forming a $C_{18}N_{28}H_{12}$ cluster. To model the effects of additional hydrogen and fluorine on this system, we investigated the effects of a single hydrogen and fluorine atom on the electronic structure of the entire cluster, treating the resulting $C_{18}N_{28}H_{13}$ and $C_{18}N_{28}H_{12}F$ systems as a doublet. The B3LYP exchange−correlation was used for both geometry optimization and TDDFT calculation of excited states. TDDFT calculations enable a rigorous calculation of the position and nature of excited states. We made use of the asymptotically corrected functional of Casida and Salahub.[37] We probed the optical absorption and the exciton distribution for both the neutral clusters and the relevant charged systems, positively charged for H and negatively charged for F.

DOI: 10.1021/acs.chemmater.6b02002
Chem. Mater. 2016, 28, 7250−7256

RESULTS AND DISCUSSION

Hybrid DFT. We first of all focus on the physical structure and binding thermodynamics of the dopants. Graphitic carbon nitride is composed of sheets of heptazine molecules (C_6N_8) linked together at their corners by C−N bonds, as shown in Figure 1, panel a. Correspondingly there are five potential sites

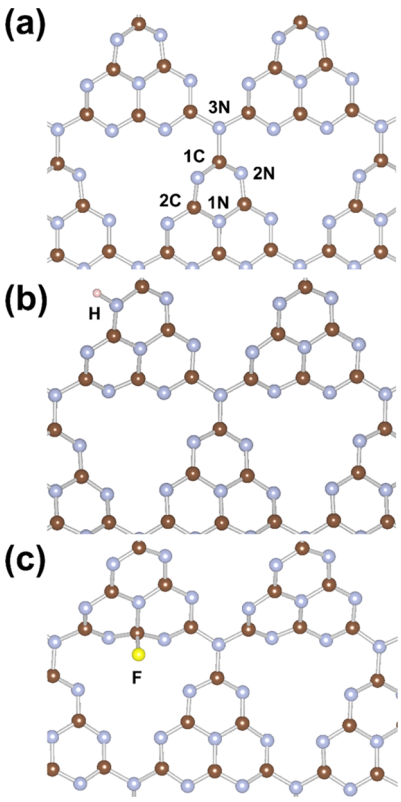

Figure 1. (a) Illustration of different potential binding sites in g-C_3N_4, (b) lowest energy structure of hydrogen doped g-C_3N_4, (c) lowest energy structure of fluorine doped structure. Light blue spheres indicate nitrogen atoms, brown spheres denote carbon atoms, pink spheres hydrogen atoms, and yellow spheres fluorine atoms.

where an atom can bind to the heptazine. These correspond to the carbon atoms on the corner (1C) and edge (2C) of the heptazine and the nitrogen atoms on the center (1N), edge (2N), and corner (3N) of the heptazine. Although each heptazine is buckled, the overall sheet structure is planar. Crystals with completely flat sheets are vibrationally stable, while sheets with buckled heptazine molecules are lower in energy by 0.32 eV. We ascribe this to the repulsive effect of the lone pair of electrons on the nitrogen atoms. This distortion is likely to enhance charge separation as suggested by Wang et al.[22] Carbon−nitrogen bonds are typically 1.32−1.33 Å, apart from the 1C−2N bond, which is 1.38 Å, and the 1C−3N bond, which is 1.46 Å. The shorter bonds indicate the delocalized π-bonds present in the heptazine molecule.

Interstitial dopant binding to all five binding sites was investigated. For hydrogen, we found that the lowest energy binding site is the 2N site of the triazine molecule, Figure 1, panel b. The next lowest site for H_i binding, the 2C site near the corner, is 1.01 eV higher in energy, with other sites 1.14 eV (3N site), 1.31 eV (1N site), and 1.51 eV higher in energy (1C site). H-interstitial binding is therefore dominated by this site. The binding of the hydrogen interstitial to the carbon nitride sheet induces a rippling with a wavelength equal to the size of the supercell. The H−N bond length is 1.03 Å, very similar to N−H bond lengths in similar systems,[38] with the hydrogen atom lying in the plane of the heptazine. The hydrogen does have an effect on the local binding of the heptazine, with the bonds adjacent to the 2N binding site lengthened by 0.03 and 0.06 Å. The hydrogen atom has perturbed the π-states that stabilize the heptazine. Furthermore, the carbon−nitrogen−carbon bond angles increase from 115.2° to 120.3°. The formation of the N−H bond reduces the nitrogen lone pair repulsion that is responsible for the buckling in the sheet. In contrast, we found that fluorine atoms have a strong tendency to bind to carbon atoms, with the lowest energy binding structure being the 2C site, see Figure 1, panel c. The carbon binding is relatively degenerate, with fluorine binding to the 1C site higher in energy by 0.15 eV. Fluorine binding to nitrogen sites 1N and 3N is unstable, with the fluorine atom relaxing to form a bond with the 1C site instead. Fluorine binding to the 2N site is stable; however, this is a structure that is 0.85 eV higher in energy. Fluorine binding is therefore dominated by the carbon site. The F−C bond length is 1.40 Å and lies perpendicular to the plane of the heptazine. Rather than residing in the open pores of the carbon nitride sheet, the fluorine prefers to reside in the interlayer spacing. The energetic driving force for this is the tendency of the fluorine atom to increase coordination. However, the fluorine atom does not insert itself into the C−N heterostructure, it is an interstitial dopant. The bonds adjacent to the 1C site are lengthened by 0.07−0.08 Å, while the local environment of the binding carbon atom is significantly changed, with N−C−N bond angles changing from 118.7°, 118.7°, and 122.6° to 111.4°, 111.8°, and 115.4°. This indicates a significant change in the electronic structure, as the local environment of the 1C site is changed from sp^2 to sp^3.

Both the hydrogen and fluorine atoms may be charged when bound to the carbon nitride lattice. Therefore, we calculate the defect formation energies for a defect α with charge q using

$$E_{\text{form}}(\alpha, q) = \Delta E(\alpha, q) + q(E_{\text{f}} - E_{\text{VBM}}) + \sum_i n_i\mu_i + E_{\text{EP}} + E_{\text{DIP}}$$

where ΔE (α, q) is the energy difference between the defect supercell and the undefected supercell, ($E_{\text{f}} - E_{\text{VBM}}$) is the energy difference between the Fermi level E_{f} and the valence band maximum E_{VBM}, μ_i is the chemical potential of elemental constituent i, of which there are n types, with corrections to the formation energy that result from the correction to the alignment of electrostatic potentials between different supercells E_{EP},[39] and E_{DIP} from the multipole interaction between dopants arising from the supercell approach.[40] These corrections are scaled by the dielectric constant of carbon nitride using the experimental value of 1.9.[41] We use the total energy of the molecular species F_2 and H_2 as the chemical potential. Our results for the formation energies of charged interstitial dopants are shown in Figure 2. In our calculations, the range of chemical potentials is chosen to range over the entire calculated bandgap (2.97 eV). Binding of the hydrogen interstitial dopant is exothermic over the entire range of chemical potentials. When the Fermi level is pinned in the middle of the band gap, we found that the lowest energy hydrogen dopant is in the +1 charge state, the hydrogen forming a proton. However, there is a charge transition level at

DOI: 10.1021/acs.chemmater.6b02002
Chem. Mater. 2016, 28, 7250−7256

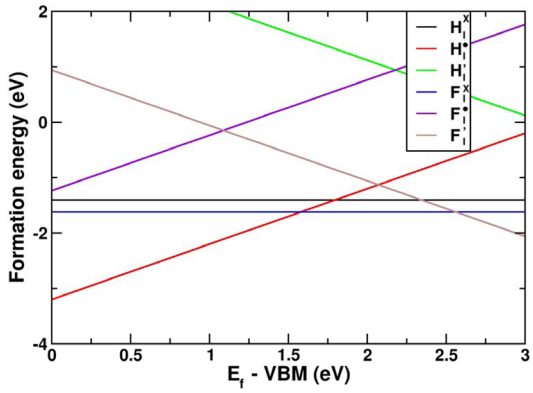

Figure 2. Defect formation energy for neutral (×), negatively charged (′), and positively charged (•) dopants, plotted for the electron chemical potential as it shifts from the VBE (left-hand side) to the CBE (right-hand side).

1.638 eV above the VBM, where the neutral hydrogen interstitial becomes preferred. Negatively charged hydrogens are not energetically favored over the permitted range of chemical potentials. A different behavior is observed for fluorine-doped systems. If the Fermi level is pinned in the middle of the bandgap then neutral fluorine interstitials are favored. Again though there is a charge transition level as the g-C_3N_4 becomes more and more n-doped, with a charge transition level to the −1 state at +2.562 eV above the Fermi level. Therefore, hydrogen doped carbon nitrides are dominated by either protons or neutral hydrogen atoms, whereas fluorine doped carbon nitrides are dominated by either neutral fluorine atoms or negative fluorine ions.

To further clarify how the dopants modify the electronic structure and thus the optical properties, we compare the DOS to ideal carbon nitride, see Figure 3. Materials with a larger bandgap will have a larger offset energy for optical absorption, which results in lower wavelength light absorption and thus

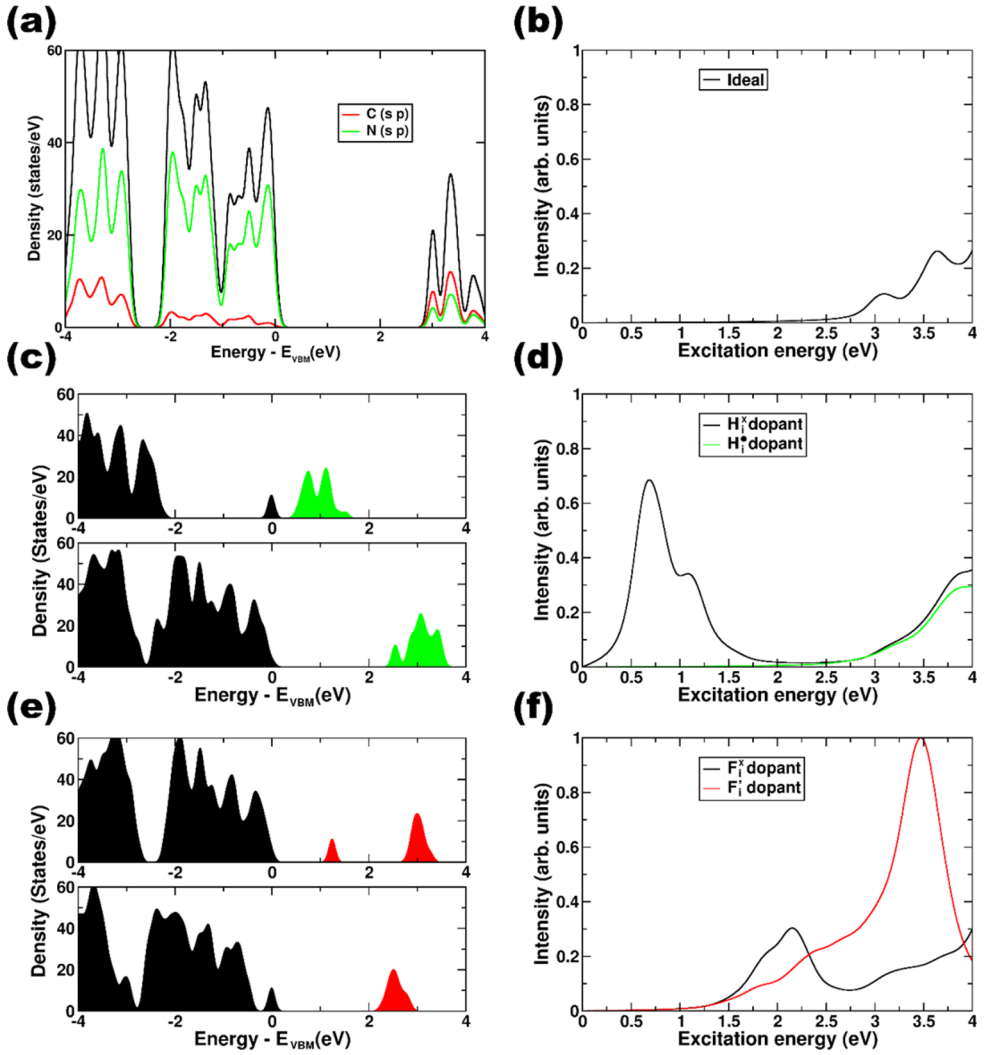

Figure 3. DOS and calculation of the absorption spectra (via determination of the imaginary dielectric function) plots for: the ideal g-C_3N_4 (a) DOS, (b) spectra; the hydrogen doped g-C_3N_4 (c) DOS with occupied states shown in black and unoccupied states shown in green for the spin-up channel of the neutral dopant (top graph) and the total spin DOS of the $H_i^•$ dopant (bottom graph), (d) spectra with the neutral interstitial shown in black and the positively charged interstitial shown in green; the fluorine doped g-C_3N_4, (e) DOS with occupied states shown in black and unoccupied states shown in red for the spin-up channel of the neutral dopant (top graph) and the total spin DOS of the F_i' dopant (bottom graph), (f) spectra with the neutral interstitial shown in black and the negatively charged interstitial shown in green. The zero of the *x*-axis of the DOS plots is set to the energy of the highest occupied state (E_{VBM}). For the optical spectra, the height of the highest intensity peak was reset to 1.0.

DOI: 10.1021/acs.chemmater.6b02002
Chem. Mater. 2016, 28, 7250−7256

poorer optical properties. For ideal bulk g-C_3N_4, our HSE06-DFT calculations find that the band gap is 2.97 eV and direct; this is an overestimate of 0.2 eV with respect to experiment.[26] From band alignment calculations, the CBE is significantly above the H^+/H redox level, while the VBE is above the OH^-/O redox level; this material can only produce hydrogen upon illumination.[26] Furthermore, the VBE is dominated by the anion sites, the nitrogen atoms. Upon hydrogenation, there is a significant reduction in the bandgap. The neutral hydrogen defect, $H_i^\times$, forms a deep donor defect with the donor state 0.54 eV below the CBE, see Figure 3. This significantly decreases the optical absorption in the spin-up channel, as can also be seen with the optical spectra. Furthermore, the binding of hydrogen to g-C_3N_4 does lead to a broadening of the bands at the VBE, which leads to a reduction in the band gap of 0.25 eV (to 2.72 eV) in the spin down channel. More significant changes occur for the positively charged hydrogen defect, $H_i^\bullet$. First, the donor state discussed previously is now empty and becomes an acceptor state. Second, the positive charge of the proton modifies the valence band, and further broadens these states and raises the valence band edge. With respect to ideal carbon nitride, the bandgap is reduced to 2.52 eV, a reduction of 0.45 eV, see Figure 3. This is primarily due to the lowering of the CBE due to the unoccupied acceptor state. The lowering of this state will reduce the thermodynamic driving force for H_2 reduction, which results in worse H_2 production kinetics. Additionally, in comparison with the predicted absorption spectra of the ideal carbon nitride, there is no major improvement in optical properties.

A different picture obtained from our analysis of the fluorine dopants likely to exist in g-C_3N_4, the neutral $F_i^\times$ and negatively charged F_i' dopants. The neutral dopant results in the formation of an acceptor state near the middle of the band gap for the spin-down channel, 1.23 eV above the VBE, see Figure 3. Furthermore, as for the hydrogen dopant, the spin-up bandgap is also reduced compared to the ideal g-C_3N_4. This arises from broadening of the valence band states due to the fluorine binding, with a reduction in band gap of 0.17 eV. Although the spin-up channel has a significantly reduced bandgap, and thus better optical absorption properties than the ideal material, in reality this dopant does not lead to better H_2 photocatalysis kinetics. There are two reasons for this, first the energy needed to split H_2O to form H_2 for an ideal system and assuming 100% efficiency is 1.23 eV. This is unlikely to be the case in a real system, where bandgaps of order 1.7 eV are regarded as optimal.[42] Second, the state in which the photoelectron will reside is significantly below the conduction band and is therefore likely to be below the H+/H redox level. There will be no thermodynamic driving force for H_2 production and thus the reaction will be kinetically and thermodynamically limited. It is a very different story for the negative dopant. The F_i' dopant manifests as a deep donor state, 0.43 eV above the VBE, see Figure 3. With the broadening of conduction band and valence band states arising from the binding of the negative interstitial, this results in a reduction in the band gap to 2.42 eV. This is a significant reduction and thus an improvement in the optical absorption properties. Indeed, in comparison with the literature, a band gap reduction of 0.55 eV is a significant improvement, whereas the largest reduction recorded is 0.21 eV. Comparison of absorption spectra for the ideal and F_i' doped materials indicates a substantially improved optical absorption at visible light energies below 3 eV (greater than 413 nm). Furthermore, the band gap reduction primarily arises from the raising of the valence band. Importantly, the proton reduction power of the negatively charged interstitial system is not reduced compared to bulk. Dopants that prefer anionic charge states will reduce the bandgap and not hinder H_2 photoproduction kinetics.

Finally, it is interesting to ask if codoping of both hydrogen and fluorine into g-C_3N_4 results in a further decrease in the bandgap and thus further improvement in the photocatalytic properties. From our analysis above, we would not expect hydrogen doping to improve H_2 production kinetics as it reduces the thermodynamic driving force for proton reduction. We modeled, using a GGA functional, the energetics and electronic structure of codoping on the same heptazine heterocycle. The lowest energy stable structure has H bound to the 2N site on one side of the heptazine and F bound to the 2C site on the other side of the heptazine. In this arrangement, we find there is very little change in the bandgap with respect to the ideal system.

TDDFT Calculations. Further insight into the effects of protonation on the effects of fluoridation or hydrogenation on the optical properties of carbon nitride can be obtained from TDDFT calculations on cluster models, specifically three trazine molecules. There is rotation of each of the triazine molecules, which results in a nonplanar structure. Since neutral hydrogen interstitials are not stable over the chemical potential range, we do not consider this defect, focusing on the proton defect, and the neutral and negatively charged fluorine defects. From inspection, we see that all of the doped models have red-shifted optical transition energies compared to the undoped cluster, with transition energies of 2.94 eV for the $H_i^\bullet$ dopant, 0.86 eV for the $F_i^\times$, and 2.12 eV for the F_i' dopant, see Figure 4. These are all significantly lower than the undoped cluster optical transition energy of 3.45 eV. In particular, the fluorine dopants have a significantly lower transition energy than the hydrogen dopant, and they push the onset for optical absorption toward the visible. Furthermore, we calculated the lowest energy exciton for all of the low energy carbon nitride models, see Figure 4. For undoped C_3N_4, the exciton is distributed relatively homogeneously over the cluster, with transitions from occupied N p_z orbitals to empty C p_z* orbitals. For the protonated cluster, there is a substantial degree of structural rearrangement, with two triazine molecules in one plane and the third perpendicular to this plane. This is not the case for the fluoridated triazines, which maintain the initial structure and thus do not strongly perturb the cluster model. From inspection of the exciton plot of the protonated cluster, there is a heterogeneous distribution of photohole density on the triazine binding to the proton and photoelectron density on the other two triazines. The majority of the exciton density is toward the center of the cluster model, which implies a stronger electrostatic interaction between photohole and photoelectron and thus a reduced recombination time. In contrast, for both of the fluoridated clusters, the fluorine-binding triazine is also the site where the photoelectron resides. There is notably less photoelectron density for the neutral fluoridated cluster than for the negatively charged fluoridated cluster, which suggests that the activity of the neutral cluster toward water reduction will be significantly less. Finally, the negatively charged fluoridated cluster has the most homogeneous exciton of all of the defect models, which suggests that this doped system will have the longest exciton recombination time of all doped systems.

DOI: 10.1021/acs.chemmater.6b02002
Chem. Mater. 2016, 28, 7250−7256

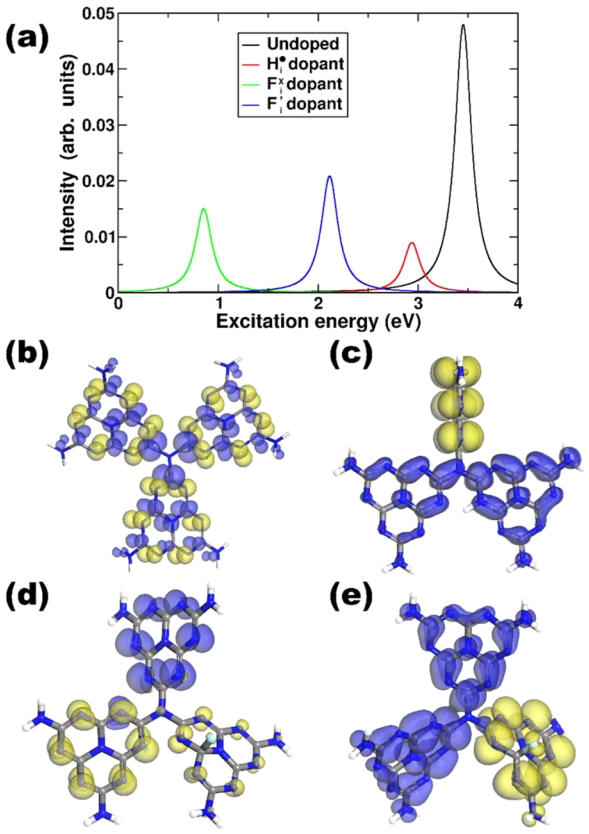

Figure 4. Excited state properties of bare and doped carbon nitride; (a) optical properties of $C_{18}N_{28}H_{12}$ (black line) and doped clusters $C_{18}N_{28}H_{13}^{+}$ (red line), $C_{18}N_{28}H_{12}F$ (green line), and $C_{18}N_{28}H_{12}F^{-}$ (blue line), the *x*-axis is labeled with respect to the HOMO state of each cluster. (b) Lowest energy exciton of $C_{18}N_{28}H_{12}$ cluster, (c) lowest energy exciton of $C_{18}N_{28}H_{13}^{+}$ cluster, (d) lowest energy exciton of $C_{18}N_{28}H_{12}F$ cluster, (e) lowest energy exciton of $C_{18}N_{28}H_{12}F^{-}$ cluster. Yellow isosurface indicates distribution of photohole upon photoexcitation, blue isosurface indicates distribution of photoelectron upon photoexcitation. Isosurfaces were plotted at 0.0005 lel/Å^3. Blue stick denotes hydrogen atoms, gray stick denotes carbon atoms, white stick denotes hydrogen atoms, and light blue stick denotes fluorine atoms.

CONCLUSIONS

We performed high quality hybrid functional DFT and TDDFT calculations on the electronic and optical properties of interstitial hydrogen and fluorine doped graphitic carbon nitrides. We have demonstrated that both elements dope exothermically into the carbon nitride lattice, with different charge states favored for different regions of the electron chemical potential. For hydrogen interstitials, the proton defect is favored for Fermi levels up to 1.64 eV above the valence band edge, while negatively charged fluorine interstitials are favored for Fermi levels greater than 2.56 eV above the valence band edge. Two separate lines of evidence indicate that these dopants significantly reduce the bandgap and thus the onset energy for optical absorption. In particular, we find that there is a 0.45 eV reduction in bandgap for $H_i^{\bullet}$ dopants and a 0.55 eV reduction in band gap for the F_i' dopant. For the latter, this pushes light absorption from 420 to 515 nm, well into the visible. Furthermore, consideration of the exciton distribution in model clusters suggests that out of all of the doped systems, anionic fluorines will result in the longest exciton recombination time. The band gap reduction mechanism differs for the two interstitial dopants, with the $H_i^{\bullet}$ lowering the conduction band edge and the F_i' dopant raising the valence band edge. Photoelectrochemically, lowering of the conduction band edge strongly reduces the thermodynamic driving force and thus efficiency of H_2 production. Proton doping is deleterious for H_2 production. The significance of our results is clear; to maximize H_2 production by bandgap reduction, it is necessary to raise the valence band. Anion dopants that raise the valence band edge are the best choice for improved H_2 photoreduction yields. Further experimental and theoretical investigation of carbon nitride photocatalysts should focus on anion doped systems to rationally design optimized metal-free photocatalysts.

AUTHOR INFORMATION

Corresponding Authors

*E-mail: s.shevlin@ucl.ac.uk.
*E-mail: z.x.guo@ucl.ac.uk.

Notes

The authors declare no competing financial interest.

ACKNOWLEDGMENTS

The authors would like to acknowledge Dr. David Scanlon, Dr. John Buckeridge, Dr. Alexey Sokol, and Dr. Junwang Tang for useful help and advice. The authors also acknowledge the use of the UCL Legion High Performance Computing Facility (Legion@UCL), the use of the IRIDIS High Performance Computing Facility, at the University of Southampton, the Grace High Performance Computing Facility (Grace@UCL), with additional compute support from the ARCHER National Computing Facility by a Resource Allocation Project (Project e454). Financial support is gratefully acknowledged from EPSRC (No. EP/L018330/1) and the EU FP7 Programme (No. 309636).

REFERENCES

(1) Fujishima, A.; Honda, K. Electrochemical Photolysis of Water at a Semiconductor Electrode. *Nature (London, U. K.)* **1972**, *238*, 37−38.
(2) Castelli, I. E.; Huser, F.; Pandey, M.; Li, H.; Thygesen, K. S.; Seger, B.; Jain, A.; Persson, K. A.; Ceder, G.; Jacobsen, K. W. New Light-Harvesting Materials Using Accurate and Efficient Bandgap Calculations. *Adv. Energy Mater.* **2015**, *5*, 1400915.
(3) Morris, C. D.; Li, H.; Jin, H.; Malliakas, C. D.; Peters, J. A.; Trikalitis, P. N.; Freeman, A. J.; Wessels, B. W.; Kanatzidis, M. G. $Cs_2M^{II}M^{IV}{}_3Q_8$ (Q = S, Se, Te): An Extensive Family of Layered Semiconductors with Diverse Band Gaps. *Chem. Mater.* **2013**, *25*, 3344−3356.
(4) Balaz, S.; Porter, S. H.; Woodward, P. M.; Brillson, L. J. Electronic Structure of Tantalum Oxynitride Perovskite Photocatalysts. *Chem. Mater.* **2013**, *25*, 3337−3343.
(5) Moniz, S. J. A.; Shevlin, S. A.; Martin, D. J.; Guo, Z.-X.; Tang, J. Visible-Light Driven Heterojunction Photocatalysts for Water Splitting - a Critical Review. *Energy Environ. Sci.* **2015**, *8*, 731−759.
(6) Sprick, R. S.; Jiang, J.-X.; Bonillo, B.; Ren, S.; Ratvijitvech, T.; Guiglion, P.; Zwijnenburg, M. A.; Adams, D. J.; Cooper, A. I. Tunable Organic Photocatalysts for Visible-Light-Driven Hydrogen Evolution. *J. Am. Chem. Soc.* **2015**, *137*, 3265−3270.
(7) Wang, X. C.; Maeda, K.; Thomas, A.; Takanabe, K.; Xin, G.; Carlsson, J. M.; Domen, K.; Antonietti, M. A Metal-Free Polymeric Photocatalyst for Hydrogen Production from Water under Visible Light. *Nat. Mater.* **2009**, *8*, 76−80.
(8) Zhang, H.; Zuo, X.; Tang, H.; Li, G.; Zhou, Z. Origin of Photoactivity in Graphitic Carbon Nitride and Strategies for Enhancement of Photocatalytic Efficiency: Insights from First-

DOI: 10.1021/acs.chemmater.6b02002
Chem. Mater. 2016, 28, 7250−7256

Principles Computations. *Phys. Chem. Chem. Phys.* **2015**, *17*, 6280−6288.
(9) Zuluaga, S.; Liu, L.-H.; Shafiq, N.; Rupich, S. M.; Veyan, J.-F.; Chabal, Y. J.; Thonhauser, T. Structural Band-Gap Tuning in G-C_3N_4. *Phys. Chem. Chem. Phys.* **2015**, *17*, 957−962.
(10) Fang, J.; Fan, H.; Li, M.; Long, C. Nitrogen Self-Doped Graphitic Carbon Nitride as Efficient Visible Light Photocatalyst for Hydrogen Evolution. *J. Mater. Chem. A* **2015**, *3*, 13819−13826.
(11) Li, J.; Shen, B.; Hong, Z.; Lin, B.; Gao, B.; Chen, Y. A Facile Approach to Synthesize Novel Oxygen-Doped G-C_3N_4 with Superior Visible-Light Photoreactivity. *Chem. Commun. (Cambridge, U. K.)* **2012**, *48*, 12017−12019.
(12) Yan, S. C.; Li, Z. S.; Zou, Z. G. Photodegradation of Rhodamine B and Methyl Orange over Boron-Doped G-C_3N_4 under Visible Light Irradiation. *Langmuir* **2010**, *26*, 3894−3901.
(13) Lin, Z.; Wang, X. Nanostructure Engineering and Doping of Conjugated Carbon Nitride Semiconductors for Hydrogen Photosynthesis. *Angew. Chem., Int. Ed.* **2013**, *52*, 1735−1738.
(14) Zhang, Y.; Mori, T.; Ye, J.; Antonietti, M. Phosphorus-Doped Carbon Nitride Solid: Enhanced Electrical Conductivity and Photocurrent Generation. *J. Am. Chem. Soc.* **2010**, *132*, 6294−6295.
(15) Ma, X.; Lv, Y.; Xu, J.; Liu, Y.; Zhang, R.; Zhu, Y. A Strategy of Enhancing the Photoactivity of G-C_3N_4 Via Doping of Nonmetal Elements: A First-Principles Study. *J. Phys. Chem. C* **2012**, *116*, 23485−23493.
(16) Hong, J.; Xia, X.; Wang, Y.; Xu, R. Mesoporous Carbon Nitride with in Situ Sulfur Doping for Enhanced Photocatalytic Hydrogen Evolution from Water under Visible Light. *J. Mater. Chem.* **2012**, *22*, 15006−15012.
(17) Liu, G.; Niu, P.; Sun, C.; Smith, S. C.; Chen, Z.; Lu, G. Q.; Cheng, H.-M. Unique Electronic Structure Induced High Photoreactivity of Sulfur-Doped Graphitic C_3N_4. *J. Am. Chem. Soc.* **2010**, *132*, 11642−11648.
(18) Wang, X.; Chen, X.; Thomas, A.; Fu, X.; Antonietti, M. Metal-Containing Carbon Nitride Compounds: A New Functional Organic-Metal Hybrid Material. *Adv. Mater. (Weinheim, Ger.)* **2009**, *21*, 1609−1612.
(19) Zhang, G. G.; Zhang, M. W.; Ye, X. X.; Qiu, X. Q.; Lin, S.; Wang, X. C. Iodine Modified Carbon Nitride Semiconductors as Visible Light Photocatalysts for Hydrogen Evolution. *Adv. Mater. (Weinheim, Ger.)* **2014**, *26*, 805−809.
(20) Wang, Y.; Zhang, J.; Wang, X.; Antonietti, M.; Li, H. Boron- and Fluorine-Containing Mesoporous Carbon Nitride Polymers: Metal-Free Catalysts for Cyclohexane Oxidation. *Angew. Chem., Int. Ed.* **2010**, *49*, 3356−3359.
(21) Wang, Y.; Di, Y.; Antonietti, M.; Li, H.; Chen, X.; Wang, X. Excellent Visible-Light Photocatalysis of Fluorinated Polymeric Carbon Nitride Solids. *Chem. Mater.* **2010**, *22*, 5119−5121.
(22) Wang, H.; Zhang, X. D.; Xie, J. F.; Zhang, J. J.; Ma, P. A.; Pan, B. C.; Xie, Y. Structural Distortion in Graphitic-C_3N_4 Realizing an Efficient Photoreactivity. *Nanoscale* **2015**, *7*, 5152−5156.
(23) Fang, J. W.; Fan, H. Q.; Zhu, Z. Y.; Kong, L. B.; Ma, L. T. ″Dyed″ Graphitic Carbon Nitride with Greatly Extended Visible-Light-Responsive Range for Hydrogen Evolution. *J. Catal.* **2016**, *339*, 93−101.
(24) Bian, J. C.; Xi, L. F.; Huang, C.; Lange, K. M.; Zhang, R. Q.; Shalom, M. Efficiency Enhancement of Carbon Nitride Photoelectrochemical Cells Via Tailored Monomers Design. *Adv. Energy Mater.* **2016**, *6*, 1600263.
(25) Cui, J.; Liang, S.; Wang, X.; Zhang, J. First Principle Modeling of Oxygen-Doped Monolayer Graphitic Carbon Nitride. *Mater. Chem. Phys.* **2015**, *161*, 194−200.
(26) Martin, D. J.; Qiu, K. P.; Shevlin, S. A.; Handoko, A. D.; Chen, X. W.; Guo, Z. X.; Tang, J. W. Highly Efficient Photocatalytic H_2 Evolution from Water Using Visible Light and Structure-Controlled Graphitic Carbon Nitride. *Angew. Chem., Int. Ed.* **2014**, *53*, 9240−9245.
(27) Kresse, G.; Furthmuller, J. Efficiency of Ab-Initio Total Energy Calculations for Metals and Semiconductors Using a Plane-Wave Basis Set. *Comput. Mater. Sci.* **1996**, *6*, 15−50.
(28) Blochl, P. E. Projector Augmented-Wave Method. *Phys. Rev. B: Condens. Matter Mater. Phys.* **1994**, *50*, 17953−17979.
(29) Perdew, J. P.; Ruzsinszky, A.; Csonka, G. I.; Vydrov, O. A.; Scuseria, G. E.; Constantin, L. A.; Zhou, X. L.; Burke, K. Restoring the Density-Gradient Expansion for Exchange in Solids and Surfaces. *Phys. Rev. Lett.* **2008**, *100*, 136406.
(30) Krukau, A. V.; Vydrov, O. A.; Izmaylov, A. F.; Scuseria, G. E. Influence of the Exchange Screening Parameter on the Performance of Screened Hybrid Functionals. *J. Chem. Phys.* **2006**, *125*, 224106.
(31) Scanlon, D. O.; Kehoe, A. B.; Watson, G. W.; Jones, M. O.; David, W. I. F.; Payne, D. J.; Egdell, R. G.; Edwards, P. P.; Walsh, A. Nature of the Band Gap and Origin of the Conductivity of PbO_2 Revealed by Theory and Experiment. *Phys. Rev. Lett.* **2011**, *107*, 246402.
(32) Zhu, J. J.; Xiao, P.; Li, H. L.; Carabineiro, S. A. C. Graphitic Carbon Nitride: Synthesis, Properties, and Applications in Catalysis. *ACS Appl. Mater. Interfaces* **2014**, *6*, 16449−16465.
(33) Reshak, A. H.; Khan, S. A.; Auluck, S. Electronic Band Structure and Specific Features of AA- and AB-Stacking of Carbon Nitride (C_3N_4): DFT Calculation. *RSC Adv.* **2014**, *4*, 6957−6964.
(34) Valiev, M.; et al. Nwchem: A Comprehensive and Scalable Open-Source Solution for Large Scale Molecular Simulations. *Comput. Phys. Commun.* **2010**, *181*, 1477−1489.
(35) Feller, D. The Role of Databases in Support of Computational Chemistry Calculations. *J. Comput. Chem.* **1996**, *17*, 1571−1586.
(36) Krishnan, R.; Binkley, J. S.; Seeger, R.; Pople, J. A. Self-Consistent Molecular-Orbital Methods 0.20. Basis Set for Correlated Wave-Functions. *J. Chem. Phys.* **1980**, *72*, 650−654.
(37) Casida, M. E.; Jamorski, C.; Casida, K. C.; Salahub, D. R. Molecular Excitation Energies to High-Lying Bound States from Time-Dependent Density-Functional Response Theory: Characterization and Correction of the Time-Dependent Local Density Approximation Ionization Threshold. *J. Chem. Phys.* **1998**, *108*, 4439−4449.
(38) Shevlin, S. A.; Kerkeni, B.; Guo, Z. X. Dehydrogenation Mechanisms and Thermodynamics of MNH_2BH_3 (M = Li, Na) Metal Amidoboranes as Predicted from First Principles. *Phys. Chem. Chem. Phys.* **2011**, *13*, 7649−7659.
(39) Freysoldt, C.; Neugebauer, J.; Van de Walle, C. G. Fully Ab Initio Finite-Size Corrections for Charged-Defect Supercell Calculations. *Phys. Rev. Lett.* **2009**, *102*, 016402.
(40) Lany, S.; Zunger, A. Assessment of Correction Methods for the Band-Gap Problem and for Finite-Size Effects in Supercell Defect Calculations: Case Studies for Zno and GaAs. *Phys. Rev. B: Condens. Matter Mater. Phys.* **2008**, *78*, 235104.
(41) Aono, M.; Nitta, S. High Resistivity and Low Dielectric Constant Amorphous Carbon Nitride Films: Application to Low-K Materials for ULSI. *Diamond Relat. Mater.* **2002**, *11*, 1219−1222.
(42) Catlow, C. R. A.; Guo, Z. X.; Miskufova, M.; Shevlin, S. A.; Smith, A. G. H.; Sokol, A. A.; Walsh, A.; Wilson, D. J.; Woodley, S. M. Advances in Computational Studies of Energy Materials. *Philos. Trans. R. Soc., A* **2010**, *368*, 3379−3456.

DOI: 10.1021/acs.chemmater.6b02002
Chem. Mater. 2016, 28, 7250−7256